Journal of Materials Chemistry A

ARTICLE

Self-Assembled Conjugated Polyelectrolyte-Surfactant Complexes as Efficient Cathode Interlayer Materials for Bulk Heterojunction Organic Solar Cells

Received 00th January 20xx,
Accepted 00th January 20xx

DOI: 10.1039/x0xx00000x

www.rsc.org/

Michèle Chevrier,[ab] Judith E. Houston,[c] Jurgen Kesters,[d] Niko Van den Brande,[e] Ann E. Terry,[f] Sébastien Richeter,[a] Ahmad Mehdi,[a] Olivier Coulembier,[b] Philippe Dubois,[b] Roberto Lazzaroni,[g] Bruno Van Mele,[e] Wouter Maes,*[d] Rachel C. Evans*[ch] and Sébastien Clément*[a]

Interfacial engineering is poised to play a key role in delivering solution-processable organic solar cells that simultaneously feature low cost and high efficiency. Here, we report the strategic design, synthesis and characterisation of phosphonium-functionalised polythiophene homo- (**P3HTPMe$_3$**) and diblock (**P3HT-*b*-P3HTPMe$_3$**) conjugated polyelectrolytes (CPEs) coupled with either bromide (Br^-) or dodecylsulfate (DS^-) surfactant counterions, for application as cathodic interlayers in polymer solar cells. The counterion is shown to have a pronounced effect on the properties of the CPEs in solution. Optical studies revealed that the bulkier DS^- counterion hinders interchain interactions more effectively, leading to a moderate blue-shift in the absorption and emission maxima. Similarly, small-angle neutron scattering (SANS) studies also indicated that the solution structures, solvent content, and therefore hydrophobicity, were extremely dependent on both the CPE structure and counterion. The effect of the CPE structure on the thermal properties of the CPE-surfactant complexes was also investigated by Rapid Heat–Cool calorimetry (RHC) measurements. CPE-DS complexes were subsequently employed as cathodic interfacial layers and shown to boost the efficiency of PBDTTPD:$PC_{71}BM$ solar cells, leading to enhanced power conversion efficiencies of 8.65% and 8.78% (on average) for **P3HTPMe$_3$,DS** and **P3HT-*b*-P3HTPMe$_3$,DS**, respectively. These values are significantly higher (~20%) than those for the corresponding device incorporating a Ca interfacial layer (7.18%), which is attributed to an increase in short-circuit current density. Atomic force microscopy studies revealed distinctions in the adhesion efficiencies of the CPE-DS complexes to the photoactive layer, which is attributed to differences in the relative hydrophobicity of the CPEs in the deposition solution.

Introduction

Photovoltaic devices are currently the subject of intense research for low-cost conversion of sunlight into electrical power.[1] In particular, solution-processed polymer solar cells, which are fabricated from the combination of an electron donor (a p-type conjugated polymer) and an electron acceptor (mainly n-type fullerene derivatives) in a bulk heterojunction structure, have emerged as a promising third-generation photovoltaic technology.[2] Although power conversion efficiencies (PCEs) now exceed 10% for single junction polymer solar cell devices, further improvement can be expected from strategic consideration and understanding of three key parameters: materials design,[3] active layer morphology,[4] and interface engineering.[5] The introduction of specific interfacial layers is commonly used to mitigate charge carrier recombination at the electrodes and thus, to improve the PCE.[6] A wide range of solution-processable materials such as metal oxides,[7] salts,[8] fullerene derivatives,[9] self-assembled monolayers of coupling agents (silanes, carboxylic acids, phosphonic acids, *etc.*)[10] and water/alcohol-soluble conjugated polymers[11] have been used for this purpose.

Conjugated polyelectrolytes (CPEs) in particular have been widely studied as interfacial charge transport and extraction layer materials.[11,12] This additional layer induces the formation and alignment of an interfacial dipole leading to a reduced work function potential of the cathode.[13-15] Improvement of

[a] *Institut Charles Gerhardt – UMR 5253, Université de Montpellier – CC1701, Place Eugène Bataillon, F-34095 Montpellier Cedex 05, France. E-mail: sebastien.clement1@umontpellier.fr; Tel: +33467143971.*
[b] *Laboratory for Polymeric and Composites Materials, Center for Innovation in Materials and Polymers, Research Institute for Science and Engineering of Materials, University of Mons – UMONS, 23 Place du Parc, B-7000 Mons, Belgium.*
[c] *School of Chemistry, Trinity College Dublin, the University of Dublin, Dublin 2, Ireland. E-mail: raevans@tcd.ie*
[d] *Institute for Materials Research (IMO), Design & Synthesis of Organic Semiconductors (DSOS), Hasselt University, Agoralaan 1–Building D, B-3590 Diepenbeek, Belgium. E-mail: wouter.maes@uhasselt.be*
[e] *Physical Chemistry and Polymer Science (FYSC), Vrije Universiteit Brussel (VUB), Pleinlaan 2, B-1050 Brussels, Belgium.*
[f] *ISIS-CCLRC, Rutherford Appleton Laboratory, Chilton, Oxon OX11 0QX, United Kingdom.*
[g] *Laboratory for Chemistry of Novel Materials, Center for Innovation in Materials and Polymers, Research Institute for Science and Engineering of Materials, University of Mons – UMONS, 23 Place du Parc, B-7000 Mons, Belgium.*
[h] *Centre for Research on Adaptive Nanostructures and Nanodevices (CRANN), Trinity College Dublin, the University of Dublin, Dublin 2, Ireland.*
†Electronic Supplementary Information (ESI) available: ^1H, $^{13}C\{^1H\}$, $^{31}P\{^1H\}$ NMR spectra; chemical structures of the photoactive layer components; SANS data analysis. See DOI: 10.1039/x0xx00000x

the operational device parameters has also been observed and attributed to a combination of enhanced charge collection, reduced charge recombination and improved and well-balanced charge carrier mobilities.[16] Orthogonal solubility with respect to the organic materials in the photoactive layer ensures sequential surface deposition without damaging the underlying films.[11,12]

CPEs exhibit significant versatility with respect to polymer structure, repeat unit, side chains, molecular weight, *etc*. This allows for strategic tailoring of the CPE structure to simultaneously modulate the optoelectronic properties, control the nanoscale film morphology and to ensure compatibility with different active layers.[16,17] Surprisingly, however, the variety of CPE structures exploited as interfacial layers to date is rather limited and is comprised mainly of thiophene- and fluorene-based (co)polymers with appended polar amine or ionic ammonium moieties.[11,12] Recently, Maes *et al.* reported that the incorporation of an imidazolium-substituted ionic polythiophene as electron transport layer in polymer solar cells leads to higher PCEs than the previously reported ammonium-functionalised ionic polythiophene.[15b] It has also been reported that donor π-conjugated cationic CPEs are optimal as cathode interface materials (thin tunneling interlayers) for organic electronic devices.[18] These findings indicate that modifying the nature of the ionic moieties in such CPEs presents a promising approach for further improvement in device performance.

In addition to the type of ionic terminal groups, the effect of the counterion must also be considered.[19] Bazan *et al.* notably reported that modification of the counterion (bromide *vs.* tetrakis(imidazolyl)borate) in a donor-acceptor based-CPE copolymer produced significant variations in the charge transport properties, ionisation potential and electron affinity.[19c] Similarly, the thermal behaviour of imidazolium-substituted polythiophenes was found to change completely when the bromide counterion was replaced by either bis(trifluoromethylsulfonyl)imide (TFSI) or hexafluorophosphate (PF_6).[20] The counterion can also play a role in controlling the ordering and orientation of the polymer and hence, enabling the orientation of the dipole moment by exploiting the electrostatic self-assembly of a CPE with a liquid crystal or surfactant molecule.[21]

Here, we report the synthesis of phosphonium-functionalised polythiophene homopolyelectrolytes and block copolyelectrolytes containing an anionic surfactant (dodecyl sulfate (DS^-)) as the counterion and demonstrate their use as cathodic interlayers to boost the internal cell parameters of polymer solar cell devices based on PBDTTPD:PC_{71}BM. We have chosen to focus on polythiophene-based CPEs due to the availability of robust synthetic protocols (*e.g*. Kumada Catalyst-Transfer Polycondensation[22]), which allow the relatively straightforward preparation of multiple polymer topographies (homopolymers, random/block copolymers) with a high degree of control over the final structure and molecular weight. Moreover, since device performance depends on both the optoelectronic properties and nanoscale morphology of the interlayer material, amphiphilic block copolyelectrolytes containing neutral and cationic polythiophene blocks can help to control the orientation and ordering of the polymer *via* solvent-induced self-assembly.[23,24] The electrostatic self-assembly of the cationic CPEs in solution is investigated using a combination of optical spectroscopy and small-angle neutron scattering (SANS). The effect of the DS^- counterion on the thermal properties of the CPE in the solid state is also examined. Finally, the incorporation of these CPE-surfactant complexes as cathodic interface layers in polymer solar cells is successfully shown to lead to improved PCEs due to an increase in the short-circuit current density (J_{sc}).

Experimental

Materials and characterisation methods

All reactions were carried out under argon or nitrogen using standard high-vacuum and Schlenk techniques. Sodium dodecyl sulfate (98.5%) was purchased from Sigma-Aldrich and used as received. All NMR spectra were recorded with a Bruker Avance III 600 MHz (^{1}H 600.26 MHz, $^{13}C\{^1H\}$ 150.96 MHz and $^{31}P\{^1H\}$ 242.98 MHz) using the solvent as the chemical shift standard, except for $^{31}P\{^1H\}$ NMR, where the chemical shifts are relative to 85% H_3PO_4 in D_2O. All chemical shifts and coupling constants are reported in ppm and Hz, respectively. Number-averaged (M_n) and weight-averaged (M_w) molecular weights and the molecular weight distributions (Đ) of the **P3HTBr** and **P3HT-*b*-P3HTBr** polymers were measured using size exclusion chromatography (SEC) on a Polymer Laboratories liquid chromatograph equipped with a PL-DG802 degasser, an isocratic HPLC pump LC 1120 (flow rate = 1 mL min^{-1}), a Marathon autosampler (loop volume = 200 µL, solution conc. = 1 mg mL^{-1}), a PL-DRI refractive index detector and three columns: a PL gel 10 µm guard column and two PL gel Mixed-B 10 µm columns (linear columns for separation of MWPS ranging from 500 to 10^6 Daltons). The eluent used was THF at a flow rate of 1 mL min^{-1} at 40 °C. Polystyrene (PS) standards were used to calibrate the SEC. The chemical composition of the CPEs was analysed using a Genesis 400 Energy Dispersive X-ray (EDX) spectrometer attached to a scanning electron microscope (Hitachi S4800 SEM).

The UV/Vis absorption and fluorescence spectra were recorded at room temperature on a Shimadzu UV2401 PC UV/Vis scanning spectrometer and a Fluorolog-3 (Horiba Jobin Yvon) spectrophotometer, respectively. The emission spectra were corrected for the wavelength response of the system using correction factors supplied by the manufacturer. Samples were measured in quartz cells with an extremely short path length (0.1 mm) to prevent saturation of the detector signal. Cyclic voltammetry (CV) was performed to investigate the electrochemical properties of the two CPEs and to obtain an estimate of their HOMO/LUMO energy levels. P3HT-like electrochemical behaviour was observed for both materials and the HOMO/LUMO values (*vide infra*) are in the same range as observed for pristine P3HT and related polythiophene-based CPEs.[15b] The electrochemical measurements were performed with an Eco ChemieAutolab

PGSTAT 30 potentiostat/galvanostat using a three-electrode microcell with a platinum wire working electrode, a platinum wire counter electrode and an anhydrous $Ag/AgNO_3$ reference electrode ($Ag/0.1$ M NBu_4PF_6 in MeCN containing 0.01 M $AgNO_3$). The CPEs were deposited onto the working electrode from methanol (**P3HTPMe$_3$,DS**) or chloroform (**P3HT-*b*-P3HTPMe$_3$,DS**) solution, to maximise solubility. The samples were analysed in anhydrous dichloromethane (**P3HTPMe$_3$,DS**) or acetonitrile (**P3HT-*b*-P3HTPMe$_3$,DS**) containing 0.1 M NBu_4PF_6. The electrolyte solution was degassed with Ar prior to each measurement. To prevent air from entering the system, a curtain of Ar was maintained during the experiments. Cyclic voltammograms were recorded at a scan rate of 100 mV s^{-1}. The HOMO energy levels were calculated from the equation E_{HOMO} (eV) = –1 X (E_{ox}^{onset} *vs.* $Ag/AgNO_3$ – $E_{Fc/Fc+}^{onset}$ *vs.* $Ag/AgNO_3$) – 4.98. The onset potentials were referenced to ferrocene/ferrocenium, which has an ionisation potential of -4.98 eV *vs.* vacuum. This correction factor is based on a value of 0.31 eV for Fc/Fc^+ *vs.* SCE[25] and a value of 4.68 eV for SCE *vs.* vacuum.[26] The LUMO energy levels were calculated from the HOMO levels and the optical bandgaps (in thin film).

SANS was carried out on the LOQ small-angle diffractometer at the ISIS Pulsed Neutron Source (STFC Rutherford Appleton Laboratory, Didcot, U.K.).[27] A simultaneous q-range of ~0.009–0.24 $Å^{-1}$ was achieved utilising an incident wavelength range of 2.2–10.0 Å separated by time-of-flight and employing a fixed sample-detector distance of 4.1 m. $q = (4\pi/\lambda)\sin(\theta/2)$ where λ is the wavelength and θ the scattering angle. Samples were prepared in deuterated methanol to provide good neutron scattering contrast. The samples were placed in quartz cuvettes (Hellma) of 1 mm path length and maintained at 25.0 ± 0.5 °C. Each raw scattering data set was corrected for the detector efficiencies, sample transmission and background scattering and converted to scattering cross-section data ($\partial\Sigma/\partial\Omega$ *vs.* q) using the instrument-specific software.[28] These data were placed on an absolute scale (cm^{-1}) using the scattering from a standard sample (a solid blend of hydrogenated and perdeuterated polystyrene) in accordance with established procedures.[29] The scattering functions were fit using non-linear least-squares analysis to a Rigid Cylinder model,[30] Flexible Cylinder model,[31] Lamellar model[32] or a Core Shell Cylinder model[33] using the SasView program. Full details of the models and the fitting procedure can be found in the Electronic Supplementary Information (ESI†).

Rapid Heat–Cool calorimetry (RHC) experiments were performed on a prototype RHC from TA Instruments, equipped with liquid nitrogen cooling and specifically designed for operation at high scanning rates,[34] using aluminium non-hermetic crucibles, and helium (10 mL min^{-1}) as a purge gas. Measurements were performed using a cooling rate of 500 K min^{-1} or 20 K min^{-1}, followed by a heating rate of 500 K min^{-1} (used to interpret the thermal transitions).

Synthesis

Poly[3-(6'-bromohexyl)thiophene-2,5-diyl] (P3HTBr). P3HTBr was prepared using Kumada Catalyst-Transfer Polycondensation according to a literature method.[35] **P3HTBr**: Yield: 73%. ^{1}H NMR ($CDCl_3$): δ = 1.39-1.59 (m, 4H, CH_2), 1.65-1.80 (m, 2H, CH_2), 1.83-1.97 (m, 2H, CH_2), 2.83 (t, 2H, CH_2, $^3J_{H-H}$ = 6 Hz), 3.43 (t, 2H, CH_2, $^3J_{H-H}$ = 6 Hz), 6.98 (s, 1H, Th) ppm. UV/Vis ($CHCl_3$): λ_{max} = 448 nm. SEC (THF, PS standards) M_n = 13,600 g mol^{-1}; Đ = 1.36.

Poly[3-hexylthiophene-2,5-diyl]-*block*-poly[3-(6'-bromohexyl)thiophene-2,5-diyl] copolymer (P3HT-*b*-P3HTBr). The KCTP method was also applied to **P3HT-*b*-P3HTBr** using our recently reported procedure.[24] The following monomer amounts were used: 2,5-dibromo-3-(6'-bromohexyl)thiophene (0.81 g, 2.00 mmol) and 2-bromo-3-hexyl-5-iodothiophene (1.07 g, 2.88 mmol). Yield: 82%. ^{1}H NMR ($CDCl_3$): δ = 0.90 (t, 3H, CH_3, $^3J_{H-H}$ = 6.8 Hz), 1.25-1.52 (m, 10H, CH_2), 1.53-1.76 (m, 4H, CH_2), 1.82-1.96 (m, 2H, CH_2), 2.80 (t, 4H, CH_2–Th, $^3J_{H-H}$ = 7.9 Hz), 3.42 (t, 2H, CH_2–Br, $^3J_{H-H}$ = 6.7 Hz), 6.98 (s, 2H, Th) ppm. UV/Vis ($CHCl_3$): λ_{max} = 451 nm; SEC (THF, PS standards): M_n = 15,100 g mol^{-1}, Đ = 1.12.

General procedure for the synthesis of P3HTPMe$_3$ and P3HT-*b*-P3HTPMe$_3$. The conversion of the bromide precursors to the desired phosphonium-functionalised polythiophenes was achieved using recent literature methods.[24,36]

P3HTPMe$_3$: Yield: 77%. ^{1}H NMR (CD_3OD): δ = 1.38-1.80 (m, 8H, CH_2), 1.94 (d, 9H, CH_3-P, $^2J_{P-H}$ = 14.5 Hz), 2.17-2.47 (m, 2H, CH_2-P), 2.79-3.02 (m, 2H, CH_2-Th), 7.13 (s, 1H, Th) ppm. $^{13}C\{^1H\}$ NMR (CD_3OD): δ = 7.4 (d, $^1J_{P-C}$ = 55 Hz), 21.5, 22.7, 23.8, 29.2, 30.5, 30.9, 129.0, 130.7, 133.9, 140.2 ppm. $^{31}P\{^1H\}$ NMR (CD_3OD): δ = 27.1) ppm. UV/Vis (MeOH): λ_{max} = 443 nm.

P3HT-*b*-P3HTPMe$_3$: Yield: 80%. ^{1}H NMR ($CDCl_3$): δ = 0.86-0.96 (m), 1.24–1.48 (m), 1.67-1.75 (m), 1.90-2.03 (m), 2.04-2.35 (br.), 2.45-2.67 (m), 2.75-2.85 (m), 6.98 (br. s) ppm. $^{13}C\{^1H\}$ NMR ($CDCl_3$): δ = 10.1 (d, $^1J_{P-C}$ = 55 Hz), 15.2, 22.8, 23.6, 23.8, 30.4, 30.2, 30.7, 31.4, 31.7, 32.7, 32.9, 129.7, 131.7, 134.8, 141.0 ppm. $^{31}P\{^1H\}$ NMR ($CDCl_3$): δ = 27.0 ppm. UV/Vis ($CHCl_3$): λ_{max} = 456 nm.

General procedure for bromide counterion exchange by dodecyl sulfate (DS). P3HTPMe$_3$ (0.100 g) or **P3HT-*b*-P3HTPMe$_3$** (0.100 g) was dissolved in demineralised water (20 mL) and a solution of sodium dodecyl sulfate (10 equivalents relative to the bromohexyl monomer) in demineralised water (10 mL) was added dropwise. The solution was stirred at room temperature for 16 h and then, poured into acetone (600 mL). The solids were filtered off, washed with acetone and dried under vacuum to give the title compounds as black solids.

P3HTPMe$_3$,DS: Yield: 86%. ^{1}H NMR (CD_3OD): δ = 0.90 (t, CH_3, $^3J_{H-H}$ = 7.0 Hz), 1.25-1.35 (m, 16H), 1.36-1.43 (m, 2H), 1.55-1.71 (m, 8H), 1.76-1.85 (m, 2H), 1.90 (d, 9H, $(CH_3)P$, $^2J_{P-H}$ = 14.5 Hz), 2.25-2.34 (m, 2H) 2.92 (br. t, 2H, $^3J_{H-H}$ = 6.0 Hz), 3.99 (t, 2H, CH_2-O-SO_3^-, $^3J_{H-H}$ = 6.5 Hz), 7.13 (s, 1H, Th) ppm. $^{13}C\{^1H\}$ NMR (CD_3OD): 8.8 (d, $^1J_{P-C}$ = 55 Hz), 15.4, 23.3, 24.6, 24.7, 25.1, 30.9, 31.3, 31.4, 31.5, 31.7, 31.8, 32.4, 32.5, 32.6, 34.0, 69.9, 131.0, 132.6, 135.8, 142.2. $^{31}P\{^1H\}$ NMR (CD_3OD): δ = 31.2 ppm. UV/Vis (MeOH): λ_{max} = 448 nm. CV (CH_2Cl_2, film): E_{HOMO} = -4.87 eV, E_{LUMO} = -2.95 eV.

P3HT-*b*-P3HTPMe$_3$,DS: Yield: 72%. ^{1}H NMR ($CDCl_3$): δ = 0.69-0.76 (m), 0.77-0.85 (m), 1.03-1.17 (m), 1.18-1.28 (m), 1.29-1.37 (m), 1.43-1.69 (m), 1.75-2.00 (m), 2.62-2.77 (m), 3.77-3.86 (m), 6.87 (s) ppm. $^{13}C\{^1H\}$ NMR ($CDCl_3$): 8.3 (d, $^1J_{P-C}$ = 55 Hz), 14.3, 14.3, 22.8, 22.9, 26.2, 29.4, 29.5, 29.6, 29.8, 29.8, 30.7, 31.9, 32.1, 53.6, 67.6, 128.8, 130.6, 133.9, 140.1 ppm. $^{31}P\{^1H\}$ NMR ($CDCl_3$): δ = 27.4 ppm. UV/Vis ($CHCl_3$): λ_{max} = 452 nm. CV (MeCN, film): E_{HOMO} = -5.10 eV, E_{LUMO} = -3.05 eV.

OPV device fabrication and characterisation

The low bandgap copolymer PBDTTPD (poly[(benzo[1,2-*b*:4,5-*b'*]dithiophene)-*alt*-(4*H*-thieno[3,4-*c*]pyrrole-4,6(5*H*)-dione)]), with 2-ethylhexyloxy and octyl side chains on the BDT and TPD units, respectively; Fig. S1, ESI†, was prepared according to a recently-developed continuous flow protocol.[37] $PC_{71}BM$ ([6,6]-phenyl-C_{71}-butyric acid methyl ester; Fig. S1, ESI†) was obtained from Solenne. Bulk heterojunction polymer solar cells were fabricated using the traditional architecture glass/ITO/PEDOT:PSS/active layer/CPE/Al. Prior to processing, the indium tin oxide (ITO; Kintec, 100 nm, 20 Ohm sq^{-1}) coated glass substrates were thoroughly cleaned using soap, demineralised water, acetone, isopropanol and a UV/O_3 treatment. PEDOT:PSS [poly(3,4-ethylenedioxythiophene):poly(styrenesulfonic acid); Heraeus Clevios] was then deposited *via* spin-coating to obtain a layer thickness of ~30 nm. Further processing was continued in a nitrogen-filled glovebox (O_2/H_2O < 0.1 ppm), initiated by a thermal treatment of 15 min at 130 °C to remove any residual water. The photoactive layer blend PBDTTPD:$PC_{71}BM$ was then spin-coated in a 1:1.5 ratio with a total concentration of 20 mg mL^{-1} from a mixture of chlorobenzene and 5% (v/v) chloronaphthalene,[38] granting an active layer thickness of ~110–120 nm. For the reference device without polyelectrolyte interlayer, Ca and Al electrodes were deposited with a thickness of ~30 and ~80 nm, respectively. For the devices employing the interlayer materials, the CPEs were spin-coated from methanol as a processing solvent in different concentrations (0.25, 0.5 and 1 mg mL^{-1}) to optimise the solar cell parameters. The thickness of the homopolymer CPE layer was 12-20 nm, while the diblock copolymer layer was 6-10 nm thick. The devices were then finished off by the deposition of ~80 nm Al as the top electrode. The *J-V* characteristics were measured using a Newport class A solar simulator (model 91195A), calibrated with a silicon solar cell to give an AM 1.5G spectrum. External quantum efficiency (EQE) measurements were performed with a Newport Apex illuminator (100 W Xenon lamp, 6257) as light source, a Newport Cornerstone 130° monochromator and a Stanford SR830 lock-in amplifier for the current measurements. The light beam was mechanically chopped at 174/149 Hz. A silicon FDS100-CAL photodiode was employed as a reference cell. For AFM imaging, a Bruker Multimode 8 AFM was used in PeakForce tapping mode, employing ScanAsyst. The images were produced with a silicon tip on a nitride lever with a spring constant of 4 N m^{-1}.

Results and discussion

Polymer synthesis

The ionic polythiophene-based homopolyelectrolyte and block copolyelectrolyte were synthesised by a two-step procedure, as recently reported by us.[24,36] First, the regioregular head-to-tail bromide-bearing polythiophene precursor polymers were prepared using KCTP polymerisation (Scheme 1).[24,35]

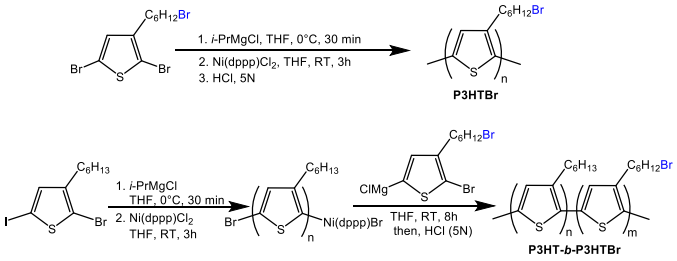

Scheme 1. Synthetic route applied towards the **P3HTBr** and **P3HT-*b*-P3HTBr** precursor polymers.

SEC analysis of the **P3HTBr** and **P3HT-*b*-P3HTBr** precursor polymers displayed a number-averaged molecular weight (M_n) of 13,600 and 15,100 g mol^{-1}, respectively, with a rather narrow dispersity (Đ = 1.36 and 1.12, respectively). The composition of the diblock copolythiophene **P3HT-*b*-P3HTBr** was determined from the ^{1}H NMR spectrum by integrating the signals observed at δ 0.90 (CH_3 groups in P3HT) and 3.42 ppm (CH_2Br groups in P3HTBr).[24] From the integration of these two signals, the molar ratio of the P3HT and P3HTBr segments was estimated to be 59:41 (feed ratio 55:45). In the next phase, the bromide precursor copolymers were converted to ionic copolymers by treatment with trimethylphosphine (Scheme 2).

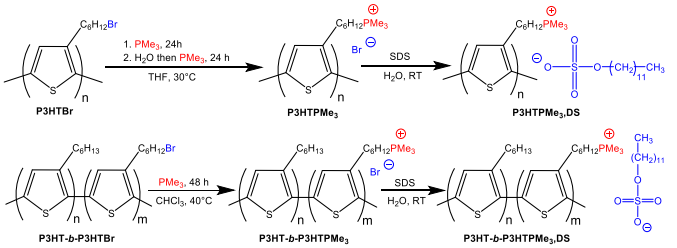

Scheme 2. Synthesis of the polyelectrolyte polymers **P3HTPMe$_3$,DS** and **P3HT-*b*-P3HTPMe$_3$,DS**.

Complete functionalisation was evidenced by the ^{1}H NMR shift of the terminal methylene group (α of the bromine) at ~3.4 ppm (in $CDCl_3$) for the bromide precursor polymers to a new one at ~2.1–2.2 ppm (in CD_3OD) attributed to the same methylene group (α of the PMe_3^+) for the ionic polymers. The incorporation of the phosphonium moieties onto the alkyl side chains of the precursor polymers is accompanied by a drastic alteration of the solubility. Compared to **P3HTBr** and **P3HT-*b*-P3HTBr**, the phosphonium-based polymer counterparts are readily soluble in DMSO, methanol and even water.

The bromide counterions in the **P3HTPMe$_3$** and **P3HT-*b*-P3HTPMe$_3$** polyelectrolytes were finally exchanged to dodecylsulfate (DS) counterions by adding a sodium dodecylsulfate (SDS) solution dropwise to the conjugated

polyelectrolytes in water (Scheme 2). The resulting solution was poured into acetone. The precipitates were filtered on a cellulose membrane, washed and dried *in vacuo*. ^{1}H NMR spectroscopy was used to determine the molar ratio between the cationic polymer and the DS^- anion (see Fig. S2 and S6, ESI†). The peaks observed at δ ~1.90 and ~3.8–3.9 ppm can be assigned to the resonance of the methyl groups linked to phosphorus in the cationic polythiophene and the methylene groups adjacent to the sulfate in the DS anion, respectively. From the integration of these two peaks, the molar ratio between the segments was found to be very close to 1:1, as expected. EDX spectroscopy confirmed that counterion exchange was quantitative since no bromine was detected.

Optical properties in solution

The optical properties of polythiophenes are well-known to be responsive to intrachain conformational changes and interchain aggregation.[39] The normalised UV/Vis absorption spectra of **P3HTPMe$_3$**, **P3HTPMe$_3$,DS**, **P3HT-*b*-P3HTPMe$_3$** and **P3HT-*b*-P3HTPMe$_3$,DS** in d_4-MeOD (10 mg mL^{-1}) are shown in Fig. 1a. The absorption maximum of the diblock copolythiophene **P3HT-*b*-P3HTPMe$_3$** is significantly red-shifted (~70 nm) compared to the homopolymer **P3HTPMe$_3$**, which is consistent with an increased aggregation of the diblock copolymer.[24] The absorption band of **P3HT-*b*-P3HTPMe$_3$** also exhibits moderate vibronic structure, which is consistent with P3HT adopting a "rigid-rod" conformation in block copolymers.[40] Counterion exchange from Br^- to DS^- results in a moderate blue-shift in the absorption maximum (~10 nm) and a narrowing of the absorption band for both polymers. **P3HT-*b*-P3HTPMe$_3$** and **P3HTPMe$_3$** also display distinct photoluminescence spectra (Fig. 1b). **P3HTPMe$_3$** exhibits a broad, featureless emission band centered at 592 nm. The emission spectrum of **P3HT-*b*-P3HTPMe$_3$** is broader still (520-850 nm) and exhibits a well-resolved vibronic structure (ΔE ≈ 0.15 eV), which is assigned to vibronic progression of the C=C stretching mode.[41] Counterion exchange from Br^- to DS^- results in the emergence of a vibronic structure for **P3HTPMe$_3$,DS** (and its further resolution for **P3HT-*b*-P3HTPMe$_3$,DS**) and moderate narrowing of the emission band.

The addition of non-ionic and ionic surfactants to CPE solutions is well-known to promote the dispersion of weakly soluble polymer aggregates by inhibiting interchain interactions, which typically manifests itself as a blue-shift in the absorption/emission maximum, narrowing of the emission band and emergence of vibronic structure.[42] We propose that for **P3HTPMe$_3$,DS** and **P3HT-*b*-P3HTPMe$_3$,DS** the DS^- counterion hinders polymer-polymer interchain interactions more effectively, thereby decreasing the nominal effective conjugation length for exciton migration.[43] Complexation of DS^- with the related homopolymers P3TMAHT[44] and P3ImiHT[45] has previously been shown to induce significant surfactochromic transitions in aqueous solution, which can be controlled by varying the surfactant fraction. However, these transitions are controlled to a large extent by the phase diagram of SDS, which differs in methanol[46] and water[47].

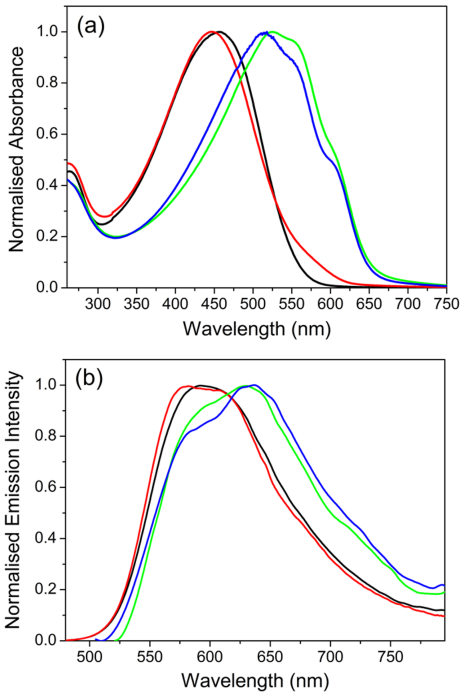

Figure 1. Normalised (a) UV/Vis absorption and (b) emission spectra of **P3HTPMe$_3$** (black line), **P3HTPMe$_3$,DS** (red line), **P3HT-*b*-P3HTPMe$_3$** (green line) and **P3HT-*b*-P3HTPMe$_3$,DS** (blue line) in d_4-MeOD (10 mg mL^{-1}).

Solution phase structure

To obtain deeper insight into the nanoscale organization of the polymers in solution, SANS studies were performed on **P3HTPMe$_3$**, **P3HTPMe$_3$,DS**, **P3HT-*b*-P3HTPMe$_3$** and **P3HT-*b*-P3HTPMe$_3$,DS** in d_4-MeOD (Fig. 2). The observation window of these SANS experiments ranged from 2.6–70 nm, which covers the isolated chain lengths of the CPEs (22.2–30.4 nm) calculated from the length of the thiophene monomer (~4 Å).[48] If the CPEs were dissolved down to the single molecule level, the SANS curve would level off as a Guinier plateau at experimentally attainable q, which is not observed here. For **P3HTPMe$_3$** the scattering profile scales as $q^{-1.22}$ in the q < 0.08 Å^{-1} region, suggesting that the homopolymer adopts a rod-like conformation in solution.[49] The corresponding Holtzer plot (q*I(q) *vs.* q, see Fig. S9a, ESI†) shows an upturn at low q (q < 0.02 Å^{-1}), which is indicative of a semi-flexible rod conformation.[50] The SANS data (0.009 < q < 0.23 Å^{-1}) were independently fit to a Rigid Cylinder model[30] (see Fig. S9b, ESI†) and a Flexible Cylinder model[31] (Fig. 2a) using a non-linear least-squares method and including q-resolution smearing. All fits are summarised in Tables S1-3 (see ESI†). The Rigid Cylinder model describes the length and radius of an unbending, uniform rod- or disc-shaped aggregate, whereas the Flexible Cylinder model is used to describe a non-linear chain consisting of a number of locally stiff segments with persistence length, l_p. The Kuhn length (L_{Kuhn}), or 2*l_p, describes the stiffness of the chain. This model gave an improved fit to the data at low q with a reasonable L_{Kuhn} (225.6 Å) compared to the total cylinder length (900.5 Å), and a radius of 12.9 Å. From the estimated aggregation number (N_{agg}), each cylinder is comprised of 5-10 polymer chains, with L_{Kuhn}

corresponding to the length of a single chain (220 Å) and the cylinder diameter (25.8 Å) approximating the thickness of two adjacent chains (~26 Å). The fitting data indicate that the cylinders are well-solvated, containing >85% solvent. Previously, the related homopolymers P3TMAHT[44] and P3ImiHT[45] in D_2O were found to form charged spherical aggregates (~80 and ~40 Å in diameter, respectively) with interparticle interaction. In contrast, **P3HTPMe$_3$** in d_4-MeOD better resembles the scattering profiles obtained from these related CPEs when combined with a small amount of DS^- (CPE/surfactant charge ratio of 1:0.2). In both systems, the pure CPE aggregates are believed to disassemble and reorganise into CPE-surfactant cylinders.[44] This suggests that **P3HTPMe$_3$** forms more ordered aggregates in d_4-MeOD, with significant packing between CPE chains.

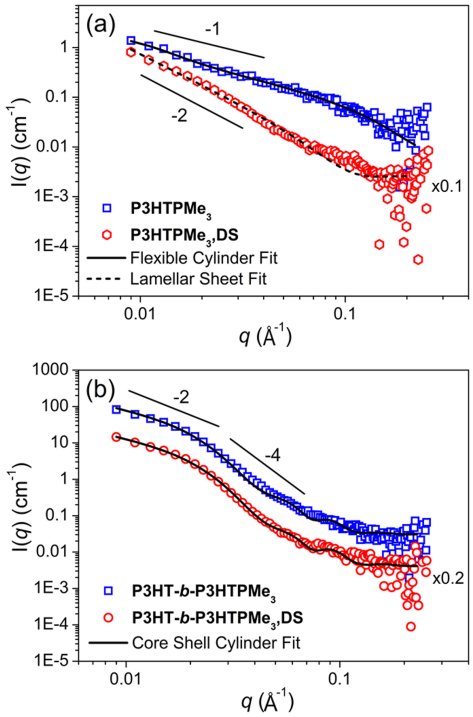

Figure 2. SANS data for (a) **P3HTPMe$_3$** (blue) and **P3HTPMe$_3$,DS** (red) and (b) **P3HT-*b*-P3HTPMe$_3$** (blue) and **P3HT-*b*-P3HTPMe$_3$,DS** (red). **P3HTPMe$_3$,DS** and **P3HT-*b*-P3HTPMe$_3$,DS** have been offset by 0.1 and 0.2 for clarity, respectively. Total concentration of each sample was 10 mg mL^{-1} in d_4-MeOD. Straight lines show -1, -2 and -4 decays for comparison. Solid and dashed lines correspond to the fits to the models described in the text.

Counterion exchange results in a significant change in the scattering profile for **P3HTPMe$_3$,DS**, scaling as $q^{-1.86}$ at low q (q < 0.02 $Å^{-1}$), and becoming steeper in the intermediate q region (0.02 < q < 0.07 $Å^{-1}$), resulting in $q^{-2.21}$, which is indicative of scattering from sheet-like particles.[49] A Lamellar Sheet model provided a reasonable fit to the data (Fig. 2a, dashed line), yielding a sheet thickness of ~47 Å, with a slightly decreased solvent content (~50%) than obtained for **P3HTPMe$_3$**. The related P3TMAHT and P3ImiHT were also found to form sheet-like aggregates when combined with a 1:1 charge ratio of SDS in H_2O.[44a,45] However, the calculated sheet thicknesses were much thinner (~20 Å), corresponding to the solid-state d-spacing of poly(3-octylthiophene) and suggesting that the sheets are formed of interwoven CPE-surfactant structures rather than well-defined layers.[48] In contrast, the sheet thickness obtained here for **P3HTPMe$_3$,DS** (~47 Å) is in excellent agreement with the sum of the length of the individual SDS molecules (~25 Å)[51] and the solid-state d-spacing of poly(3-octylthiophene), suggesting that distinct DS^-/CPE layers are present. However, due to the similar scattering length densities (SLDs) for **P3HTPMe$_3$** and DS^- (~1 × 10^{-6} $Å^{-2}$), the individual layers cannot be distinguished by this experiment. Nevertheless, the formation of sheet-like, rigid particles does suggest more efficient packing of the CPE within lamellar sheets, potentially leading to the exclusion of d_4-MeOD molecules and hence the lower solvent content.

The SANS data of **P3HT-*b*-P3HTPMe$_3$** in d_4-MeOD (see Fig. 2b) yield a similar scattering profile to the pyridinium (Py) and imidazolium (Im) **P3HT-*b*-P3HTX** analogues previously studied in d_4-MeOD and D_2O.[24] The scattering data exhibit a shoulder at q = 0.02 $Å^{-1}$ and an upturn at q = 0.08 $Å^{-1}$. At high q (q > 0.07 $Å^{-1}$), the SANS response stems from the internal structure of the aggregate. The low q region (q < 0.02 $Å^{-1}$) decays as $q^{-1.8}$, which is typical of scattering from either cylindrical aggregates or from individual chains.[49] The SANS data were fit to a Core-Shell Cylinder model, as previously described.[33] **P3HT-*b*-P3HTPMe$_3$** aggregates fit to a dry core (~15% solvent) with a radius (r_{core}) of 53.1 Å, length (L_{core}) of 572.8 Å, and a thick, wet shell (~86% solvent) of 77.4 Å. Each aggregate contains ~300 chains. The SLDs of the neutral P3HT and the $P3HTPMe_3$ blocks are both ~1 × 10^{-6} $Å^{-2}$. Therefore they can only be distinguished by neutron scattering when one block is substantially more solvated than the other. A difference in solubility between amphiphilic copolymer blocks is known to lead to the formation of domains within CPE aggregates.[23b] Here, we observe core-shell cylinders with hydrophobic, neutral block cores and solvated, hydrophilic charged block shells. It should be noted that the phosphonium analogue appears to have a wetter and thicker shell than the Py and Im analogues previously studied.[24] This result is in good agreement with the significantly larger hydrodynamic diameter obtained by dynamic light scattering for **P3HT-*b*-P3HTPMe$_3$** in comparison to the Py and Im analogues.[24]

Counterion exchange yields only subtle changes in the scattering profile for **P3HT-*b*-P3HTPMe$_3$,DS**, with the core-shell cylinder structure of the parent copolymer retained (Fig. 2b). The power law scaling for the intermediate q region varies from $q^{-4.39}$ for the parent diblock to $q^{-4.93}$ for **P3HT-*b*-P3HTPMe$_3$,DS**, suggesting a slight change in the internal aggregate morphology. Fitting with the Core-Shell Cylinder model gave moderately elongated cylinder cores, L_{core} = 544.4 Å and r_{core} = 54.3 Å, with a slightly drier shell (~85% solvent) with a shell thickness, T_{shell} = 74.0 Å. The core is slightly more solvated (~19%) than the parent **P3HT-*b*-P3HTPMe$_3$**, which may explain the difference in q-scaling of the intermediate region. The shell thickness for the CPE with and without DS^- remains almost constant. The surfactant is expected to associate parallel to the CPE chains extending from the hydrophobic block core. This is consistent with the slightly lower N_{agg} ~230 obtained for **P3HT-*b*-P3HTPMe$_3$,DS**. As such,

we do not expect an increase in the thickness of the CPE shell, only in the chain packing/density within the shell, which is suggested by the subtle decrease in 'wetness'. Unfortunately, the similarity between the SLDs of the CPE block and surfactant means that we can only observe the 'global' shell structure. Future studies will involve contrast matching with d_{25}-DS^- to try and pin-point the exact orientation of the CPEs within the CPE,DS complexes. Nevertheless, we can conclude that DS^- counterion exchange has only a limited effect on the solution structure of **P3HT-*b*-P3HTPMe$_3$,DS**, with the hydrophobic P3HT core apparently retaining the cylindrical morphology of the pure diblock. In comparison, the less-aggregated homopolymer **P3HTPMe$_3$** is able to freely transform from semi-flexible cylinders to rigid sheets upon counterion exchange.

Thermal behaviour

An RHC study was performed on **P3HTPMe$_3$,DS** and **P3HT-*b*-P3HTPMe$_3$,DS** to investigate thermal transitions occurring in the solid-state (Fig. 3). Results were found to be reproducible after an initial heating which removes thermal history. When a fast cooling rate of 500 K min^{-1} is employed, the homopolymer **P3HTPMe$_3$,DS** shows a clear glass transition (T_g) at about 70 °C, followed by cold crystallisation and a melting transition. As no crystallisation is observed during the cooling, it can be concluded that a fast cooling rate leads to an amorphous material before the onset of cold crystallisation. A slower cooling rate of 20 K min^{-1}, allowing crystallisation to take place during cooling, was therefore used to obtain more information about the crystallisation process. Such a treatment leads to a much more pronounced melting transition, which takes the form of a main melting peak with a peak maximum of 152 °C, and a smaller shoulder at 176 °C. Due to the higher crystalline fraction, the glass transition is hardly visible in this case. These results seem to indicate that the **P3HTPMe$_3$,DS** polymer exhibits rather slow crystallisation kinetics, in contrast to P3HT which is known to exhibit fast crystallisation kinetics.[52]

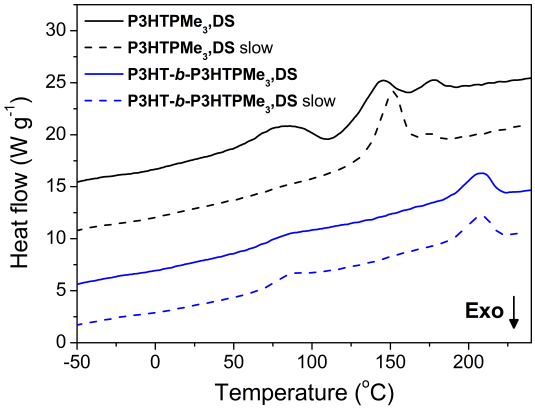

Figure 3. RHC thermograms of **P3HTPMe$_3$,DS** and **P3HT-*b*-P3HTPMe$_3$,DS** at 500 K min^{-1} heating rate, for a preceding cooling rate of either 500 K min^{-1} (solid lines) or 20 K min^{-1} (dashed lines). These thermograms correspond to the reproducible second heating, after erasing the thermal history in the first heating.

The **P3HT-*b*-P3HTPMe$_3$,DS** block copolymer exhibits different thermal behaviour, with a glass transition at about 70 °C, followed by a clear melting peak at 206 °C. While a glass transition temperature of 70 °C can be linked to the **P3HTPMe$_3$,DS** block, the melting point is clearly higher. Furthermore, the crystallisation process is much faster, leading to a clear melting peak and a complete absence of cold crystallisation after cooling at 500 K min^{-1}. For comparison, a slower cooling rate of 20 K min^{-1} was also employed, leading to a similar thermogram. Based on these results it seems this crystallisation and melting can be attributed to the P3HT block. As P3HT crystallisation is a faster process which takes place at higher temperatures, it will also hinder crystallisation of the **P3HTPMe$_3$,DS** block. A separate glass transition for the P3HT block is not observed, which can be explained by the high crystallinity of the P3HT block. Similar behaviour was previously reported for a **P3HT-*b*-P3HTPMe$_3$,Br** copolymer, where P3HT crystallisation was also dominant and the same melting point was observed.[24] Furthermore, taking into account a total M_n of 15,100 g mol^{-1}, and a molar ratio of 0.59 for the P3HT block, the observed melting point of 206 °C seems to fit with earlier P3HT results for different molecular weights.[53] We note that T_g and T_m will depend on all experimental conditions (synthetic sequence, block ratio, M_n, Đ, purification, drying, storage, *etc.*). However, the lower T_g observed for both **P3HTPMe$_3$,DS** and **P3HT-*b*-P3HTPMe$_3$,DS**, compared to the Br^- analogues,[24] indicates the role of the DS^- in increasing the free volume due to its size. An increase in free volume for a similar temperature can be directly linked to a lower T_g. This is in agreement with the observed trends for the optical properties in solution, where DS^- hinders chain aggregation. In addition, the flexible unit of the DS^- counterion may also enhance the plasticising effect. This has previously been observed when SDS was used as an emulsifier.[54] Furthermore, a decrease in the T_g due to the plasticising effect of a counterion was also seen for bis(trifluoromethanesulfonyl)imide ($TFSI^-$).[20]

Photovoltaic properties

To investigate the behaviour of the CPEs containing anionic DS surfactants as cathodic interlayers, bulk heterojunction polymer solar cells with traditional architecture (glass/ITO/PEDOT:PSS/PBDTTPD:$PC_{71}BM$/CPE/Al) were fabricated. The photoactive layer PBDTTPD:$PC_{71}BM$ (1:1.5), chosen for its high and reproducible performance,[37,38] was deposited from a combination of chlorobenzene and 5% (v/v) chloronaphthalene as the processing solvent. The CPE interlayers were then spin-coated directly on top of the photoactive layer from methanol solutions in various concentrations (0.25, 0.5 and 1 mg mL^{-1}) to optimise the final device performance. As summarised in Table 1 and Fig. 4, the incorporation of the surfactant interlayers mostly affects the J_{sc},[15b] resulting in significantly improved (*ca.* 20%) PCEs, from an average value of 7.18 to 8.65 and 8.78% for the homopolymer and block copolymer surfactants, respectively (for an interlayer concentration of 0.5 mg mL^{-1}). These values are significantly higher than reported for polymer solar cells

Table 1. Photovoltaic performance of PBDTTPD:$PC_{71}BM$ polymer solar cells with and without the incorporation of **P3HTPMe$_3$,DS** or **P3HT-*b*-P3HTPMe$_3$,DS** cathode interfacial layers.[a]

Cathodic interlayer	Concentration (mg mL^{-1})	V_{oc} (V)	J_{sc} (mA cm^{-2})	FF	Average PCE (%)[b]	Best PCE (%)
Ca		0.93	11.32	0.69	7.18	7.70
\ (Methanol)		0.92	11.73	0.71	7.69	7.89
P3HTPMe$_3$,DS	0.25	0.93	12.52	0.70	8.15	8.49
P3HTPMe$_3$,DS	0.5	0.93	13.20	0.70	8.65	8.83
P3HTPMe$_3$,DS	1	0.95	13.30	0.68	8.60	8.77
P3HT-*b*-P3HTPMe$_3$,DS	0.25	0.93	12.97	0.70	8.41	8.78
P3HT-*b*-P3HTPMe$_3$,DS	0.5	0.93	13.52	0.70	8.78	8.91
P3HT-*b*-P3HTPMe$_3$,DS	1	0.95	12.75	0.68	8.24	8.26

[a] Device structure: glass/ITO/PEDOT:PSS/PBDTTPD:$PC_{71}BM$/Ca or CPE/Al. [b] Average over 4–8 devices.

incorporating a P3TMAHT-DS complex as a cathodic interlayer (PCE = 4.01% for P3HT:$PC_{61}BM$ and PCE = 6.47% for PTB7:$PC_{71}BM$).[21b] A control device with pure methanol spin-coated on top of the photoactive layer also provided some efficiency increase (7.69% average, 7.89% best PCE), in accordance with previous findings,[15b,17c,55] but the obtained values were still significantly below the PCEs observed upon incorporation of the CPE interlayers.

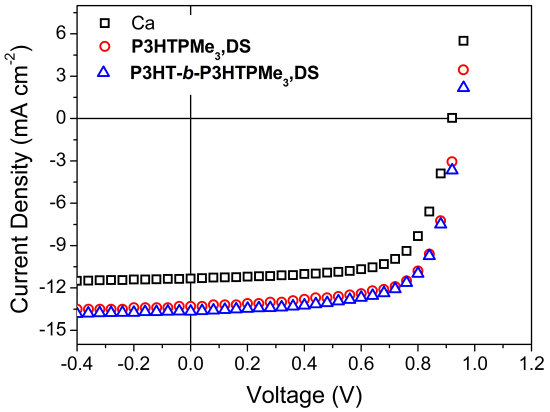

Figure 4. *J-V* curves for average performance PBDTTPD:$PC_{71}BM$ solar cell devices produced with and without CPE interlayers (0.5 mg mL^{-1} deposition solution).

From the EQE spectra, enhanced photocurrent generation over the entire absorption range can be observed upon incorporation of the surfactant interlayers (Fig. 5). A maximum EQE of 65% was obtained for the reference device, whereas this increased to ~80% for the devices with CPE cathodic interlayers. The extracted current densities from the EQE measurements (J_{EQE} = 13.06 and 13.39 mA cm^{-2} for the **P3HTPMe$_3$,DS** and **P3HT-*b*-P3HTPMe$_3$,DS** interlayers, respectively) correspond well to the measured J_{sc} values, in accordance with standard measurement deviations.

AFM measurements were performed to investigate the adhesion efficiency of the two DS surfactant-based interfacial materials to the PBDTTPD:$PC_{71}BM$ photoactive layer. As illustrated in Fig. 6, a distinctly different topography can be observed for the homo and block polyelectrolytes, both granting non-complete active layer coverage after spin-coating. However, while **P3HT-*b*-P3HTPMe$_3$,DS** shows an improved affinity towards deposition on top of the photoactive layer, this phenomenon does not seem to have a major influence on the final device performance.

The solution-phase structure of the casting solution is expected to affect the morphology of the subsequently deposited layer. However, in this case we do not see a direct correlation between the solution structure observed by SANS and the AFM topography. It should be noted that the SANS experiments are performed at significantly higher solution concentrations than employed for film deposition (~10x larger), which could account for this difference, most notably the absence of extended structures. Moreover, spin-coating is known to reduce the crystallinity of P3HT thin films as it prevents appropriate alignment of the polymer chains.[56] Thermally-induced morphological instability due to the formation of non-equilibrium structures during device operation is also a consideration.[57] A detailed study is now underway to determine the key relationships between the solution structure, film deposition process and film structure and morphology which underpin the significant enhancement in the PCEs observed here.

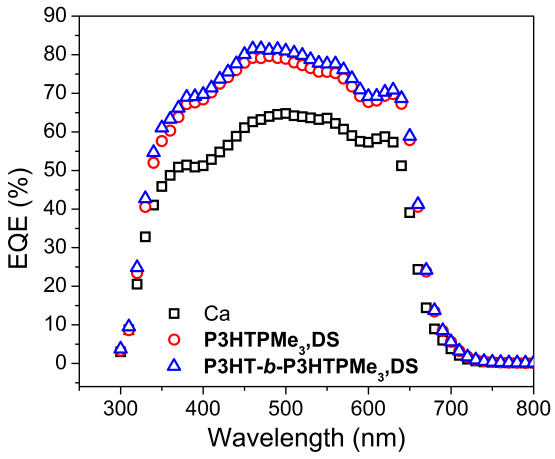

Figure 5. EQE spectra for average performance PBDTTPD:$PC_{71}BM$ solar cell devices with and without CPE interlayers (0.5 mg mL^{-1} deposition solution).

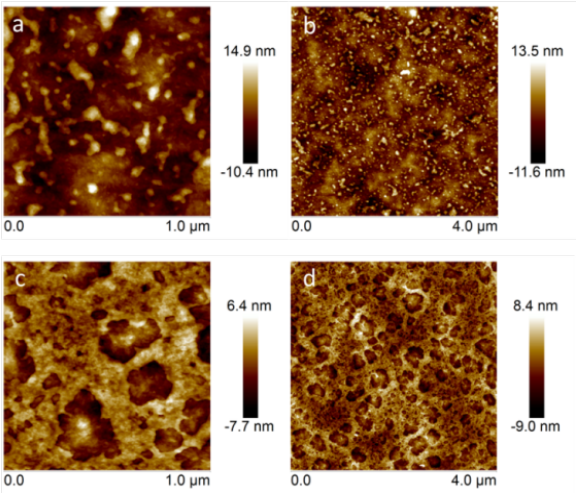

Figure 6. AFM (topography) images (1 x 1 µm and 4 x 4 µm) of **P3HTPMe$_3$,DS** (a,b) and **P3HT-*b*-P3HTPMe$_3$,DS** (c,d) on top of the PBDTTPD:PC$_{71}$BM photoactive layer.

Conclusions

Phosphonium-functionalised polythiophene homopolyelectrolytes and block copolyelectrolytes containing either bromide or dodecylsulfate as the counterion have been successfully synthesised using the KCTP method. The optical properties of **P3HTPMe$_3$** and **P3HT-*b*-P3HTPMe$_3$** in methanolic solution show a moderate dependence on the nature of the counterion, with the bulkier DS^- ion leading to a small blue shift in the absorption and emission maxima. This is attributed to reduced interchain interactions, and thus, a decrease in the effective conjugation length, driven by the presence of the larger counterion. SANS studies reveal that **P3HTPMe$_3$**(Br^-/DS^-) and **P3HT-*b*-P3HTPMe$_3$**(Br^-/DS^-) exhibit significantly different structures in solution. While **P3HTPMe$_3$,Br** adopts a flexible rod-like conformation with a high solvent content, **P3HTPMe$_3$,DS** favours a lamellar-type structure believed to be comprised of distinct **P3HTPMe$_3$** and DS^- layers. In contrast, both **P3HT-*b*-P3HTPMe$_3$** and **P3HT-*b*-P3HTPMe$_3$,DS** form core-shell cylindrical aggregates in solution, with the P3HT block comprising the core and the P3HTPMe$_3$ block (and associated counterions) forming the aggregate shell. Thermal analysis of **P3HTPMe$_3$,DS** reveals that it exhibits slow crystallisation kinetics and a glass transition at ~70 °C. In contrast, **P3HT-*b*-P3HTPMe$_3$,DS** displays a clear thermal signature of the diblock architecture, with a T_g caused by the CPE block and a T_m associated with the P3HT block. **P3HT-*b*-P3HTPMe$_3$,DS** exhibits significantly faster crystallisation kinetics than the corresponding homopolymer, which is attributed to the intrinsic tendency of the P3HT block towards crystallisation. **P3HTPMe$_3$,DS** and **P3HT-*b*-P3HTPMe$_3$,DS** have been successfully employed as cathodic interfacial layers to enhance the efficiency of PBDTTPD:PC$_{71}$BM solar cells, leading to optimised average PCEs of 8.65% and 8.78%, respectively. This is an improvement of >20% compared to the corresponding device incorporating a Ca interfacial layer and is attributed to an increase in J_{sc}. AFM studies revealed differences in the adhesion efficiencies of **P3HTPMe$_3$,DS** and **P3HT-*b*-P3HTPMe$_3$,DS** to the photoactive layer. However, the enhanced coverage observed for **P3HT-*b*-P3HTPMe$_3$,DS** does not lead to any significant enhancement in the photovoltaic performance. The successful use of **P3HTPMe$_3$,DS** and **P3HT-*b*-P3HTPMe$_3$,DS** as cathodic interface layers highlights the crucial role that interfacial engineering must play to break the prevailing paradigm and finally achieve low cost and high performance in parallel. Given the vast tunability offered by CPEs, coupled with their solution processability, it can be expected that continuing developments in the strategic structural design of these materials will have an important part to play in delivering this goal.

Acknowledgements

This work was supported by CNRS and the Université de Montpellier. This work was supported in part by Science Foundation Ireland under Grant No. 12/IP/1608. Research in Mons is supported by the FNRS-FRFC and Région Wallonne (OPTI^{2}MAT excellence programme). The authors are also grateful to the National Fund for Scientific Research (F.R.S.-FNRS) in the frame of the FRFC research programme (convention No. 2.4508.12). The University of Mons and Hasselt University co-authors are grateful for financial support by the Science Policy Office of the Belgian Federal Government (BELSPO; PAI/IAP 7/05). The HINT COST action MP1202 and French–Irish program ''Hubert Curien Ulysses'' (31998ZF) are acknowledged for support. This research has been supported by the European Commission under the 7th Framework Programme through the 'Research Infrastructures' action of the 'Capacities' programme. Contract no: CP-CSA_INFRA-2008-1.1.1 Number 226507-NM13. We thank ISIS and STFC for the allocation of SANS Xpress beamtime.

References

1 (a) M.-E. Ragoussi and T. Torres, *Chem. Commun.*, 2015, **51**, 3957; (b) H. Youn, H. J. Park and L. J. Guo, *Small*, 2015, **11**, 2228; (c) S. Roland, S. Neubert, S. Albrecht, B. Stannowski, M. Seger, A. Facchetti, R. Schlatmann, B. Rech and D. Neher, *Adv. Mater.*, 2015, **27**, 1262; (d) *Organic Photovoltaics: Materials, Device Physics, and Manufacturing Technologies*, 2nd Edition, ed. C. Brabec, U. Scherf and V. Dyakonov, Wiley-VCH, Weinheim, 2014.

2 (a) I. Burgues-Ceballos, M. Stella, P. Lacharmoise and E. Martinez-Ferrero, *J. Mater. Chem. A*, 2015, **2**, 17711; (b) R. Po, A. Bernardi, A. Calabrese, C. Carbonera, G. Corso and A. Pellegrino, *Energy Environ. Sci.*, 2014, **7**, 925; (c) Y. Sun, Y. Zhang, Q. Liang, Y. Zhang, H. Chi, Y. Shi and D. Fang, *RSC Adv.*, 2013, **3**, 11925; (d) G. Li, R. Zhu and Y. Yang, *Nat. Photon*., 2012, **6**, 153.

3 (a) E. Zhou, K. Hashimoto and K. Tajima, *Polymer*, 2013, **54**, 6501; (b) H. Zhou, L. Yang and W. You, *Macromolecules*, 2012, **45**, 607; (c) Y. Li, *Acc. Chem. Res.*, 2012, **45**, 723; (d) C. L. Chochos and S. A. Choulis, *Prog. Polym. Sci.*, 2011, **36**, 1326.

4 (a) M. He, M. Wang, C. Lin and Z. Lin, *Nanoscale*, 2014, **6**, 3984; (b) T. Wang, A. J. Pearson and D. G. Lidzey, *J. Mater.*

Chem. C, 2013, **1**, 7266; (c) R. Noriega, J. Rivnay, K. Vandewal, F. P. V. Koch, N. Stingelin, P. Smith, M. F. Toney and A. Salleo, *Nat. Mater.*, 2013, **12**, 1038; (d) W. Cai, X. Gong and Y. Cao, *Sol. Energy. Mater. Sol. Cells*, 2010, **94**, 114.

5 (a) H. Zeng, X. Zhu, Y. Liang and X. Guo, *Polymers*, 2015, **7**, 333; (b) G. Liu, S. Ji, G. Xu and C. Ye, *Pure Appl. Chem.*, 2012, **84**, 2653; (c) L.-M. Chen, Z. Xu, Z. Hong and Y. Yang, *J. Mater. Chem.*, 2010, **20**, 2575.

6 (a) R. Po, C. Carbonera, A. Bernardi and N. Camaioni, *Energy Environ. Sci.*, 2011, **4**, 285; (b) T.-H. Lai, S.-W. Tsang, J. R. Manders, S. Chen and F. So, *Mater. Today*, 2013, **16**, 424.

7 (a) S. Chen, J. R. Manders, S.-W. Tsang and F. So, *J. Mater. Chem.*, 2012, **22**, 24202; (b) J. Y. Kim, S. H. Kim, H.-H. Lee, K. Lee, W. Ma, X. Gong and A. J. Heeger, *Adv. Mater.*, 2006, **18**, 572; (c) M. Vasilopoulou, E. Polydorou, A. M. Douvas, L. C. Palilis, S. Kennou and P. Argitis, *Energy Environ. Sci*., 2015, **8**, 2448.

8 (a) S. K. M. Jonsson, E. Carlegrim, F. Zhang, W. R. Salaneck and M. Fahlman, *Jpn. J. Appl. Phys.*, 2005, **44**, 3695; (b) C. J. Brabec, S. E. Shaheen, C. Winder, N. S. Sariciftci and P. Denk, *Appl. Phys. Lett.*, 2002, **80**, 1288.

9 (a) C.-Z. Li, C. C. Chuch, H.-L. Yip, K. M. O'Malley, W.-C. Chen and A. K.-Y. Jen, *J. Mater. Chem.*, 2012, **22**, 8574; (b) C. Duan, C. Zhong, C. Liu, F. Huang and Y. Cao, *Chem. Mater.*, 2012, **24**, 1682.

10 (a) C. K. Song, K. A. Luck, N. Zhou, L. Zeng, H. M. Heitzer, E. F. Manley, S. Goldman, L. X. Chen, M. A. Ratner, M. J. Bedzyk, R. P. H. Chang, M. C. Hersam and T. J. Marks, *J. Am. Chem. Soc.*, 2014, **136**, 17762; (b) S. Das, J. Joslin and T. L. Alford, *Sol. Energy. Mater. Sol. Cells*, 2014, **124**, 98; (c) H. Wang, J. M. Mativetsky, Y. Ren, E. D. Gomez, C. Jaye, J. Schwartz, D. A. Fischer and Y.-L. Loo, *Org. Electron.*, 2014, **15**, 3333; (d) H. Choi, J. Lee, W. Lee, S.-Y. Ko, R. Yang, J. C. Lee, H. Y. Woo, C. Yang and J. Y. Kim, *Org. Electron.*, 2013, **14**, 3138; (e) M. Song, J.-W. Kang, D.-H. Kim, J.-D. Kwon, S. G. Park, S. Nam, S. Jo, S. Y. Ryu and C. S. Kim, *Appl. Phys. Lett.*, 2013, **102**, 143303/1; (f) T. Stubhan, M. Salinas, A. Ebel, F. C. Krebs, A. Hirsch, M. Halik and C. J. Brabec, *Adv. Energy Mater.*, 2012, **2**, 532

11 (a) Z. Hu, K. Zhang, F. Huang and Y. Cao, *Chem. Commun.*, 2015, **51**, 5572; (b) Z. He, H. Wu and Y. Cao, *Adv. Mater.*, 2014, **26**, 1006; (c) C. Duan, K. Zhang, C. Zhong, F. Huang and Y. Cao, *Chem. Soc. Rev.*, 2013, **42**, 9071.

12 W. Lee, J. H. Seo and H. Y. Woo, *Polymer*, 2013, **54**, 5104.

13 C. He, C. M. Zhong, H. B. Wu, R. Q. Yang, W. Yang, F. Huang, G. C. Bazan and Y. Cao, *J. Mater. Chem.*, 2010, **20**, 2617.

14 (a) M. Y. Jo, Y. E. Ha, Y. S. Wonb, S. I. Yoo and J. H. Kim, *Org. Electron.*, 2015, **25**, 85; (b) H. B. Wu, F. Huang, Y. Q. Mo, W. Yang, D. L. Wang, J. B. Peng and Y. Cao, *Adv. Mater.*, 2004, **16**, 1826; (c) H. B. Wu, F. Huang, J. B. Peng and Y. Cao, *Org. Electron.*, 2005, **6**, 118.

15 (a) J. Drijkoningen, J. Kesters, T. Vangerven, E. Bourgeois, L. Lutsen, D. Vanderzande, W. Maes, J. D'Haen and J. Manca, *Org. Electron.*, 2014, **15**, 1282; (b) J. Kesters, T. Ghoos, H. Penxten, J. Drijkoningen, T. Vangerven, D. M. Lyons, B. Verreet, T. Aernouts, L. Lutsen, D. Vanderzande, J. Manca and W. Maes, *Adv. Energy Mater.*, 2013, **3**, 1180.

16 (a) Z. C. He, C. Zhang, X. F. Xu, L. J. Zhang, L. Huang, J. W. Chen, H. B. Wu and Y. Cao, *Adv. Mater.*, 2011, **23**, 3086; (b) R. C. Evans, *J. Mater. Chem. C*., 2013, **1**, 4190.

17 (a) W. Vanormelingen, J. Kesters, P. Verstappen, J. Drijkoningen, J. Kudrjasova, S. Koudjina, V. Liégeois, B. Champagne, J. Manca, L. Lutsen, D. Vanderzande and W. Maes, *J. Mater. Chem. A,* 2014, **2**, 7535; (b) H. Choi, J. S. Park, E. Jeong, G. H. Kim, B. R. Lee, S. O. Kim, M. H. Song, H. Y. Woo and J. Y. Kim, *Adv. Mater.*, 2011, **23**, 2759; (c) J. H. Seo, A. Gutacker, Y. M. Sun, H. B. Wu, F. Huang, Y. Cao, U. Scherf, A. J. Heeger and G. C. Bazan, *J. Am. Chem. Soc.*, 2011, **133**, 8416; (d) Z. C. He, C. M. Zhong, X. Huang, W. Y. Wong, H. B. Wu, L. W. Chen, S. J. Su and Y. Cao, *Adv. Mater.*, 2011, **23**, 4636.

18 Q. Bao, X. Liu, E. Wang, J. Fang, F. Gao, S. Braun and M. Fahlman, *Adv. Mater. Interfaces*, 2015, **2**, 1500204.

19 (a) A. Garcia, J. Z. Brzezinski and T.-Q. Nguyen, *J. Phys. Chem C*, 2009, **113**, 2950; (b) M. Kang, O. K. Nag, R. R. Nayak, S. Hwang, H. Suh and H. Y. Woo, *Macromolecules*, 2009, **42**, 2708; (c) Z. B. Henson, Y. Zhang, T.-Q. Nguyen, J. H. Seo and G. C. Bazan, *J. Am. Chem. Soc.*, 2013, **135**, 4163; (d) D. Tordera, M. Kuik, Z. D. Rengert, E. Bandiello, H. J. Bolink, G. C. Bazan and T.-Q. Nguyen, *J. Am. Chem. Soc.*, 2014, **136**, 8500.

20 T. Ghoos, J. Brassinne, C.-A. Fustin, J.-F. Gohy, M. Defour, N. Van den Brande, B. Van Mele, L. Lutsen, D. J. Vanderzande and W. Maes, *Polymer*, 2013, **54**, 6293.

21 (a) L. Chen, C. Xie and Y. Chen, *Macromolecules*, 2014, **47**, 1623; (b) Y.-M. Chang, R. Zhu, E. Richard, C.-C. Chen, G. Li and Y. Yang, *Adv. Funct. Mater.*, 2012, **22**, 3284.

22 (a) P. Sista and C. K. Luscombe, in *P3HT Revisited – From Molecular Scale to Solar Cell Devices*, Advances in Polymer Science, ed. S. Ludwigs, Springer-Verlag, Berlin, Heidelberg, 2014, vol. 265, pp. 1; (b) T. Yokozawa, Y. Nanashima and Y. Ohta, *ACS Macro Lett*., 2012, **1**, 862; (c) M. C. Stefan. M. P. Bhatt, P. Sista and H. D. Magurudeniya, *Polym. Chem*., 2012, **3**, 1693; (d) I. Osaka and R. D. McCullough, *Acc. Chem*. *Res*., 2008, **41**, 1202.

23 (a) G. Tu, H. Li, M. Forster, R. Heiderhoff, L. J. Balk, R. Sigeland and U. Scherf, *Small*, 2007, **3**, 1001; (b) A. Gutacker, S. Adamczyk, A. Helfer, L. E. Garner, R. C. Evans, S. M. Fonseca, M. Knaapila, G. C. Bazan, H. D. Burrows and U. Scherf, *J. Mater. Chem.*, 2010, **20**, 1423; (c) A. Gutacker, N. Koenen, U. Scherf, S. Adamczyk, J. Pina, S. M. Fonseca, A. J. M. Valente, R. C. Evans, J. Seixas de Melo, H. D. Burrows and M. Knaapila, *Polymer*, 2010, **51**, 1898; (d) M. Knaapila, R. C. Evans, A. Gutacker, V. M. Garamus, M. Torkkeli, S. Adamczyk, M. Forster, U. Scherf and H. D. Burrows, *Langmuir*, 2010, **26**, 5056.

24 A. Thomas, J. E. Houston, N. Van den Brande, J. De Winter, M. Chevrier, R. K. Heenan, A. E. Terry, S. Richeter, A. Mehdi, B. Van Mele, P. Dubois, R. Lazzaroni, P. Gerbaux, R. C. Evans and S. Clément, *Polym. Chem.*, 2014, **5**, 3352.

25 A. J. Bard and L. R. Faulker, in *Electrochemical Methods: Fundamentals and Applications,* John Wiley and Sons, New York, 2nd edn, 2001.

26 S. Trasatti, *Pure Appl. Chem*., 1986, **58**, 955.

27 R. K. Heenan, J. Penfold and S. M. King, *J. Appl. Crystallogr.*, 1997, **30**, 1140.

28 http://www.mantidproject.org

29 G. D. Wignall and F. S. Bates, *J. Appl. Crystallogr*., 1987, **20**, 28.

30 A. Guinier and G. Fournet, in *Small-Angle Scattering of X-Rays*, ed. John Wiley and Sons, New York, 1955.

31 (a) W.-R. Chen, P. D. Butler and L. J. Magid, *Langmuir*, 2006, **22**, 6548; (b) J. S. Pederson and P. Schurtenberger, *Macromolecules*, 1996, **29**, 7602.

32 (a) J. Berghausen, J. Zipfel, P. Lindner and W. Richtering, *J. Phys. Chem. B*, 2001, **105**, 11081; (b) F. Nallet, R. Laversanne and D. Roux, *J. Phys. II France*, 1993, **3**, 487.

33 I. Livsey, *J. Chem. Soc., Faraday Trans. 2*, 1987, **83**, 1445.

34 (a) R. L. Danley, P. A. Caulfield and S. R. Aubuchon, *Am. Lab.,* 2008, **40**, 9; (b) S. Wouters, F. Demir, L. Beenaerts and G. Van Assche, *Thermochim. Acta.,* 2012, **530**, 64.

35 S. Clément, A. Tizit, S. Desbief, A. Mehdi, J. De Winter, P. Gerbaux, R. Lazzaroni and B. Boury, *J. Mater. Chem.*, 2011, **21**, 2733.

36 J. Rubio-Magnieto, A. Thomas, S. Richeter, A. Mehdi, P. Dubois, R. Lazzaroni, S. Clément and M. Surin, *Chem. Commun.*, 2013, **49**, 5483.
37 G. Pirotte, J. Kesters, P. Verstappen, S. Govaerts, J. Manca, L. Lutsen, D. Vanderzande and W. Maes, *ChemSusChem*., 2015, **8**, 3228.
38 (a) Y. Zou, A. Najari, P. Berrouard, S. Beaupré, B. R. Aïch, Y. Tao and M. Leclerc, *J. Am. Chem. Soc.*, 2010, **132**, 5330; (b) C. Cabanetos, A. El Labban, J. A. Bartelt, J. D. Douglas, W. R. Mateker, J. M. J. Fréchet, M. D. McGehee and P. M. Beaujuge, *J. Am. Chem. Soc.*, 2013, **135**, 4656; (c) J. A. Bartelt, J. D. Douglas, W. R. Mateker, A. El Labban, C. J. Tassone, M. F. Toney, J. M. J. Fréchet, P. M. Beaujuge and M. D. McGehee, *Adv. Energy Mater.*, 2014, **4**, 1301733.
39 (a) K. K. Stokes, K. Heuzé and R. D. McCullough, *Macromolecules*, 2003, **36**, 7114; (b) K. Faïd, M. Fréchette, M. Ranger, L. Mazerolle, I. Lévesque, M. Leclerc, T.-A. Chen and R. D. Rieke, *Chem. Mater.*, 1995, **7**, 1390.
40 Y.-H. Lee, W.-C. Yen, W.-F. Su and C.-A. Dai, *Soft Matter*, 2011, **7**, 10429.
41 M. Sundberg, O. Inganäs, S. Stafström, G. Gustafsson and B. Sjögren, *Solid State Commun.,* 1989, **71**, 435.
42 (a) H. D. Burrows, M. J. Tapia, S. M. Fonseca, S. Pradhan, U. Scherf, C. L. Silva, A. A. C. C. Pais, A. J. M. Valente, K. Schillén, V. Alfredsson, A. M. Carnerup, M. Tomšič and A. K. Jamnik, *Langmuir*, 2009, **25**, 5545; (b) M. J. Tapia, H. D. Burrows, A. J. M. Valente, S. Pradhan, U. Scherf, V. M. M. Lobo, J. Pina and J. Seixas de Melo, *J. Phys. Chem. B*, 2005, **109**, 19108.
43 H. D. Burrows, V. M. M. Lobo, J. Pina, M. L. Ramos, J. Seixas de Melo, A. J. M. Valente, M. J. Tapia, D. Pradham and U. Scherf, *Macromolecules*, 2004, **37**, 7425.
44 (a) M. Knaapila, R. C. Evans, V. M. Garamus, L. Almäsy, N. K. Székely, A. Gutacker, U. Scherf and H. D. Burrows, *Langmuir*, 2010, **26**, 15634; (b) R. C. Evans, M. Knaapila, N. Willis-Fox, M. Kraft, A. Terry, H. D. Burrows and U. Scherf, *Langmuir*, 2012, **28**, 12348.
45 M. Knaapila, R. C. Evans, A. Gutacker, V. M. Garamus, N. K. Székely, U. Scherf and H. D. Burrows, *Soft Matter*, 2011, **7**, 6863.
46 A. I. Mitsionis and T. C. Vaimakis, *Chem. Phys. Lett*., 2012, **547**, 110.
47 P. Kekicheff, C. Grabielle-Madelmont and M. Ollivon, *J. Colloid Inter. Sci.,* 1989, **131**, 112.
48 T. J. Prosa, M. J. Winokur, J. Moulton, P. Smith and A. J. Heeger, *Macromolecules*, 1992, **25**, 4364.
49 P. W. Schmidt, in *Some Fundamental Concepts and Techniques Useful in Small-Angle Scattering Studies of Disordered Solids. In Modern Aspects of Small-Angle Scattering*, ed. H. Brumberger, Kluwer Academic Publishers, Dordrecht, The Netherlands, 1995, pp 1-56.
50 S. R. Kline, *Langmuir*, 1999, **15**, 2726.
51 N. A. Mazer, G. B. Benedek, and M. C. Carey, *J. Phys. Chem*., 1976, **80**, 1075.
52 N. Van den Brande, G. Van Assche and B. Van Mele, *Polymer*, 2015, **57**, 39.
53 D. Spoltore, T. Vangerven, P. Verstappen, F. Piersimoni, S. Bertho, K. Vandewal, N. Van den Brande, M. Defour, B. Van Mele, A. De Sio, J. Parisi, L. Lutsen, D. Vanderzande, W. Maes and J. V. Manca, *Org. Electron*., 2015, **21**, 160.
54 N. Grossiord, H. E. Miltner, J. Loos, J. Meuldijk, B. Van Mele and C. E. Koning, *Chem. Mater*., 2007, **19**, 3787.
55 H. Zhou, Y. Zhang, J. Seifter, S. D. Collins, C. Luo, G. C. Bazan, T.-Q. Nguyen and A. J. Heeger, *Adv. Mater*., 2013, **25**, 1646.
56 H. Erothu, J. Kolomanska, P. Johnston, S. Schumann, D. Deribew, D. T. W. Toolan, A. Gregori, C. Dagron-Lartigau, G. Portale, W. Bras, T. Arnold, A. Distler, R. C. Hiorns, P. Mokarian-Tabari, T. W. Collins, J. R. Howse and P. D. Topham, *Macromolecules*, 2015, **48**, 2107.
57 R. Dattani, J. H. Bannock, Z. Fei, R. C. I. MacKenzie, A. A. Y. Guilbert, M. S. Vezie, J. Nelson, J. C. de Mello, M. Heeney, J. T. Cabral and A. J. Nedoma, *J. Mater. Chem. A*, 2014, **2**, 14711.